Journal of the Meteorological Society of Japan, Vol. 91, No. 4, pp. 471–488, 2013
DOI:10.2151/jmsj.2013-404

Potential Impact of Sea Surface Temperature on Winter Precipitation over the Japan Sea Side of Japan: A Regional Climate Modeling Study

Hiroshi G. TAKAHASHI

Japan Agency for Marine-Earth Science and Technology, Yokohama, Japan and Graduate School of Urban Environmental Sciences, Tokyo Metropolitan University, Japan

Noriko N. ISHIZAKI, Hiroaki KAWASE, Masayuki HARA, Takao YOSHIKANE, Xieyao MA, and Fujio KIMURA

Japan Agency for Marine-Earth Science and Technology, Yokohama, Japan

(Manuscript received 29 November 2012, in final form 27 March 2013)

Abstract

In this study, a regional climate model (WRF-ARW; the Advanced Research Weather Research and Forecasting model) having a resolution of 4.5 km was used to examine the sensitivity of precipitation on the Japan Sea side of Japan to the sea surface temperature (SST) in the Japan Sea during winter. We performed a control simulation (CTL) driven by reanalysis and observational SST datasets. Three sensitivity experiments in which SSTs over the entire domain were 1K, 2K, and − 1K different from the CTL SST were conducted to examine the sensitivity of precipitation to SST. The calculated precipitation on the Japan Sea side increased by 6–12% K^{-1} of SST warming. Concurrent with the precipitation changes, latent heat flux over the Japan Sea increased by 11–14% K^{-1} of SST warming. Because the changes in surface relative humidity were very small, the increase can be explained by the Clausius–Clapeyron equation. The deviation from the 7% increase in latent heat flux calculated from this equation can be quantitatively explained by the development of the planetary boundary layer over the Japan Sea, which was related to an increase in sensible heat flux due to the SST warming. This result also implies that the 1 K uncertainty in simulated and projected SST over the Japan Sea among multiple atmosphere–ocean global climate models corresponds to an approximately 10% uncertainty in precipitation on the Japan Sea side of Japan.

Keywords sea of Japan; winter monsoon; SST; sensitivity; uncertainty

1. Introduction

Climate change can significantly influence the snowfall on the Japan Sea side of Japan because the seasonal surface air temperature is higher than 0°C. This side of Japan is one of the heaviest snowfall regions on Earth. These heavy snowfalls are a consequence of the northwesterly flow of the Asian winter monsoon from Eurasia and the region's windward (northwestern side) position along Japan's northeast–southwest trending central mountain range (Fig. 1). Two main factors influence precipitation over the Japan Sea side. One is the activity of cold and dry northwesterly winds of the Asian winter monsoon, and the other is sensible and latent heat fluxes on the Japan Sea, which are strongly associated with the sea surface

Corresponding author: Hiroshi G. Takahashi, Japan Agency for Marine-Earth Science and Technology, Yokohama, Japan and Graduate School of Urban Environmental Sciences, Tokyo Metropolitan University, Japan, 3173-25, Showa-machi, Kanazawa-ku, Yokohama-city, Kanagawa 236-0001, Japan
E-mail: hiroshi3@tmu.ac.jp

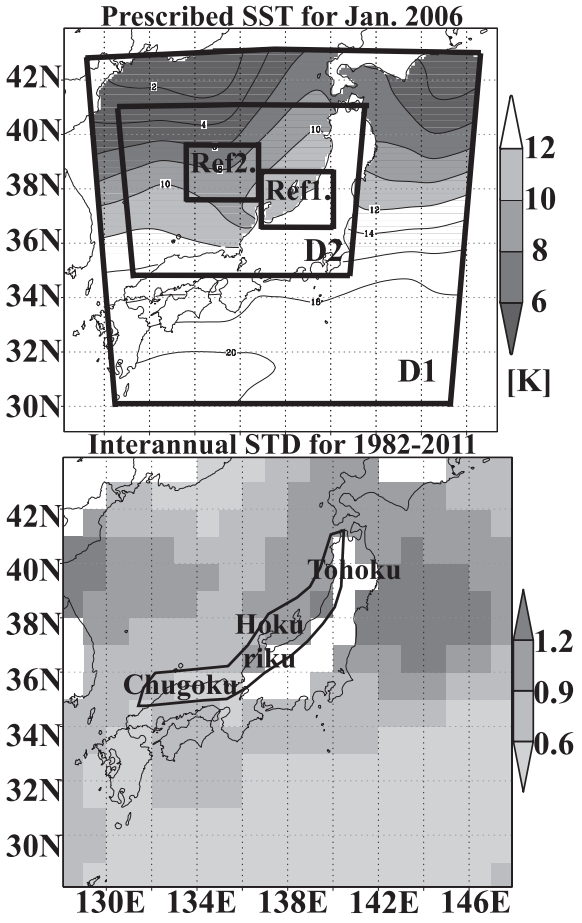

Fig. 1. (a) Calculation domain (D1 and D2) and prescribed SST. The SST was interpolated on a model grid from the original OISST. Reference regions 1 and 2, which were used for obtaining the area-averaged physical values, are shown. (b) Interannual standard deviation of SST from 1982 to 2011. Land areas in OISST are masked. The area encircled by the black solid line is the Japan Sea side of Japan.

temperature (SST). To understand the past and future climate changes in this region, the potential of each of these factors in modulating precipitation must be quantified.

The Siberian High over Eurasia produces cold, dry air masses that moisten as they flow across the Japan Sea. This wet monsoon flow brings considerable precipitation to the Japan Sea side of Japan (e.g., Manabe 1957, 1958). An observational study showed a positive correlation between snowfall over the Japan Sea side and heat flux in the Tsushima Warm Current (Hirose and Fukudome 2006). Takano et al. (2008) suggested that the SST played a role in a particularly heavy snowfall event in December 2005, although anomalous atmospheric circulation was primarily significant. Recently, Takahashi and Idenaga (2013) revealed that the warmer SST over the Japan Sea is probably associated with higher precipitation on the Japan Sea side of Japan from the observational data. In this region, it is possible that SST controls the precipitation. This study aims to quantify the impact of SST on precipitation on the Japan Sea side of Japan.

Previous studies examined the impact of increased SST along the Japan Sea coast using regional climate models with a horizontal resolution of 10 or 20 km and suggested that spatially high-resolution SST data can improve the simulation of atmospheric circulation and precipitation (Yamamoto and Hirose 2008, 2009; Iizuka 2010). They also found that warmer SST results in increased precipitation over the Japan Sea side of Japan. However, these experiments changed not only the spatial SST distribution but also the mean SSTs, implying that the effects of both were included in the results. Thus, although valuable for realistic simulation, the sensitivity of precipitation to SST is difficult to estimate by their approach. In addition, the spatial resolution of the models was too coarse to simulate basic precipitation systems in the region, such as the development of cloud streaks over the Japan Sea and precipitation associated with a complex terrain. Few regional climate simulations of sensitivity of precipitation on the Japan Sea side to SST have been conducted by using high-resolution models.

In addition, uncertainties must be reduced for quantitative projection of future regional climate (Hawkins and Sutton 2009). Projections of future regional climate obtained by downscaling from various atmosphere–ocean global climate models (AOGCMs) disagree in some regions, and the uncertainties of projections should be evaluated (Christensen et al. 2007). One goal of this study was to quantify the uncertainty in simulated precipitation on the Japan Sea side of Japan, which is associated with the SST in the Japan Sea.

Using high-resolution experiments, we quantitatively examined the sensitivity of precipitation on the Japan Sea side to SST in the Japan Sea. Our focus was on the sensitivity of precipitation to mean SST and not on the effects of the spatial distribution of SST. We also considered the physical mechanism that determines this sensitivity. By quantitatively examining the influence of uncertainty in SST on uncertainty in simulated precipitation, this study contributes to efforts to model future climate in the study region.

2. Data and numerical experiment

To understand the potential impact of SST in the Japan Sea on precipitation over the Japan Sea side of Japan, we conducted numerical experiments using a non-hydrostatic regional climate model, the Advanced Research Weather Research and Forecasting (WRF) modeling system (Skamarock et al. 2008) Version 3.3. For initial and boundary conditions, we used the atmosphere from the National Centers for Environmental Prediction (NCEP) Final Operational Model Global Tropospheric Analyses (FNL) and SST from the Optimized Interpolated SST V2 (OISST; Reynolds et al. 2002). The Japan Sea side of Japan was selected as the computational target region. The model domains are shown in Fig. 1. A portion of the Hokuriku District (Niigata and Toyama prefectures), one of the heaviest snowfall areas, was selected as the reference region to examine the changes in precipitation (Fig. 1). We conducted three 1-month control time-slice experiments (CTL) for a winter monsoon season extending from December to February. We selected the three months of December 2005, January 2006, and February 2006 as the simulation periods, representing a typical winter heavy-snowfall season in the recent decade. These simulation periods extend from 29 November 2005 to 1 January 2006, from 30 December 2005 to 1 February 2006, and from 30 January 2006 to 1 March 2006, respectively. The first two days of each simulation were not used for analysis but as a spin-up period. Because the SST condition in these experiments was fixed at the initial values for simplification of the experimental design, a positive bias in the simulated precipitation, compared with a result considering temporal SST changes was expected (SST in the Japan Sea decreases gradually with time in winter). To reduce the expected positive bias, we conducted the 1-month experiments separately. The horizontal grid increment of the coarse domain was 18 km and that of the two-way nested domain was 4.5 km. Both domains had 27 terrain-following vertical levels. We performed 4.5-km resolution experiments because Hara et al. (2008), Ma et al. (2010), and Yoshikane et al. (2011) showed that simulated precipitation from a horizontal resolution finer than 5 km agreed with the observations.

Moreover, because cumulus convective parameterization (CCP) controls not only convective systems but also the related atmospheric circulation through thermodynamics effects, sensitivity experiments may depend almost exclusively on CCP. Because test simulations with CCP showed an unrealistic amount of precipitation, we did not apply CCP in either domain. The Mellor–Yamada–Nakanishi–Niino Level 2.5 planetary boundary layer scheme (Nakanishi and Niino 2004), the WRF single-moment six-class microphysics scheme (Hong and Lim 2006), the Noah land-surface model (Chen and Dudhia 2001), the Rapid Radiative Transfer Model (RRTM) longwave radiation scheme (Mlawer et al. 1997), and Dudhia shortwave radiation scheme (Dudhia 1989) were used.

To understand the impact of SST, we conducted three sensitivity experiments for December 2005, January 2006, and February 2006. The numerical design of these experiments was the same as that of CTL, except that the SST over the entire domain was changed by +1, +2, and −1 K compared to CTL. These conditions are hereafter referred to as SST+1K, SST + 2K, and SST − 1K, respectively. The range of SST changes in the sensitivity experiments was determined with reference to that of the interannual variations in the observed SST (Fig. 1). The interannual standard deviation of the monthly mean SST for January over a 30-year period was approximately 1 K over the Japan Sea.

In total, we conducted 12 experiments driven by FNL and OISST as the initial and boundary conditions (i.e., CTL and three sensitivity experiments for each of the three months). Twelve other experiments were conducted using a different set of initial and boundary conditions to confirm the robustness of the sensitivity of precipitation to SST. The results of the latter set of experiments are given in Appendix A.

We used two precipitation datasets to evaluate the simulated precipitation. One was the daily precipitation amount from the Automated Meteorological Data Acquisition System (AMeDAS) from the Japan Meteorological Agency (JMA), which is a point-based dataset. The other was a grid-based precipitation dataset referred to as APHRODITE-JP (Aphro; Kamiguchi et al. 2010). The spatial resolution in longitude and latitude of Aphro was 0.05°.

3. Results

3.1 Evaluation of CTL

To understand the impact of SST on precipitation over the Japan Sea side of Japan, we first evaluated the spatial distribution of the simulated precipitation. As illustrated in Fig. 2, AMeDAS and Aphro observations showed abundant precipitation over southern Niigata Prefecture from the coast to the mountainous regions (around 138°E, 37°N). The spatial distribution of the Aphro precipitation did not indicate the detailed spatial structure shown by AMeDAS, but the large-scale

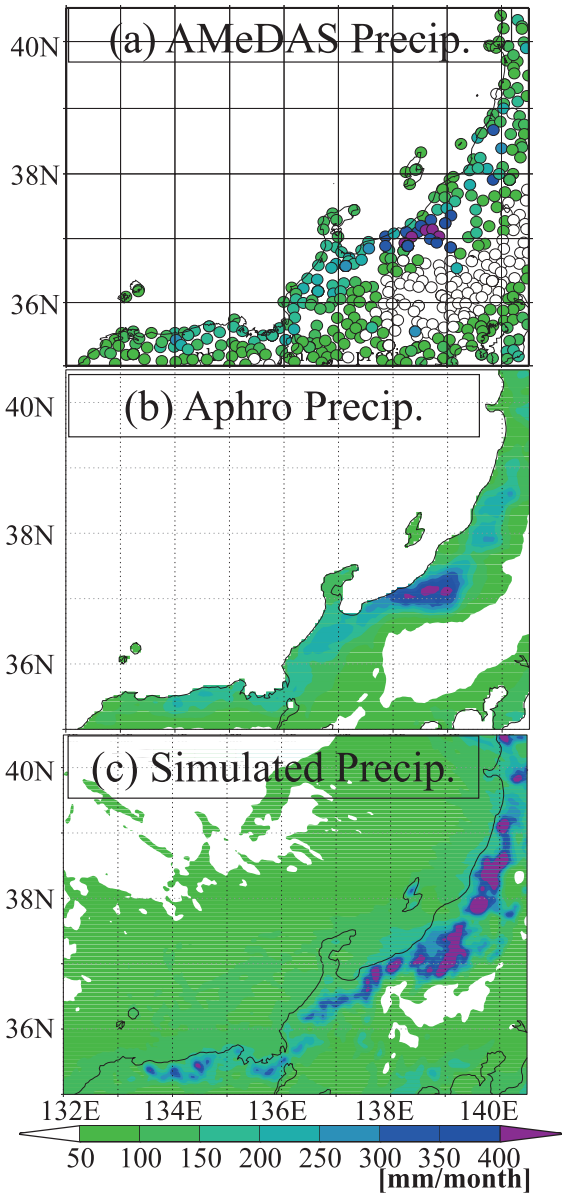

Fig. 2. (a) Observed AMeDAS, (b) observed Aphro, and (c) simulated monthly precipitation in January 2006. The simulated precipitation is the sum of liquid and solid precipitations. The unit is millimeters per month.

pattern of the Aphro precipitation was similar to that of AMeDAS. The peaks of the simulated precipitation correlated closely with the peaks indicated by observations. For December 2005 and February 2006, the spatial distributions of the simulated precipitation were also similar to those of the observed precipitation (not shown). Most snapshots of precipitation and

Table 1. Simulated and two types of observed monthly precipitation over the land in reference region 1 (137–140°E, 36.5–38.5°N; shown in Fig. 1) expressed in mm/month. Simulated and Aphro precipitations were area-averaged over reference region 1. Available AMeDAS observations, which have less than 10% missing values, were averaged in reference region 1. The numbers of stations used for the average values are shown in parentheses in the AMeDAS column.

	CTL	Obs (Aphro)	Obs (AMeDAS)
DEC2005	358.2	351.8	360.0 (91)
JAN2006	230.4	167.1	172.5 (92)
FEB2006	198.6	148.9	148.3 (94)

atmospheric circulation patterns obtained from CTL reproduced typical cloud streaks over the Japan Sea (not shown), indicating that our experiments captured basic precipitation systems over the region.

We also evaluated the seasonal progression of precipitation over reference region 1 (Fig. 1) by comparing the observed and simulated monthly averaged precipitation over the region (Table 1). The seasonal progression of the simulated monthly mean precipitation on the Japan Sea side agreed with that of the observed monthly mean precipitation. The simulated precipitation was the highest in December 2005; both observed and simulated values in December 2005 were higher than the precipitation amount in January and February 2006. The amounts of precipitation in January and February were basically the same for the observations and the simulation. These results imply that the relative seasonal changes in the precipitation from the simulation and observations were also very similar. Therefore, precipitation was realistically simulated in these experiments, although the absolute values of simulated precipitation were comparable to or somewhat larger than the observed precipitation values in all months. Note that both simulated and observed precipitation can include individual biases.

3.2 Sensitivity of precipitation to SST

Three sensitivity experiments using the same initial and boundary conditions, except for SST, were separately conducted for December 2005, January 2006, and February 2006. The differences between CTL and SST + 1K for January 2006 are shown in Fig. 3. These differences in precipitation were in good agreement with the differences between SST + 1K and SST + 2K and between SST − 1K and CTL. In addition, similar results were obtained from the

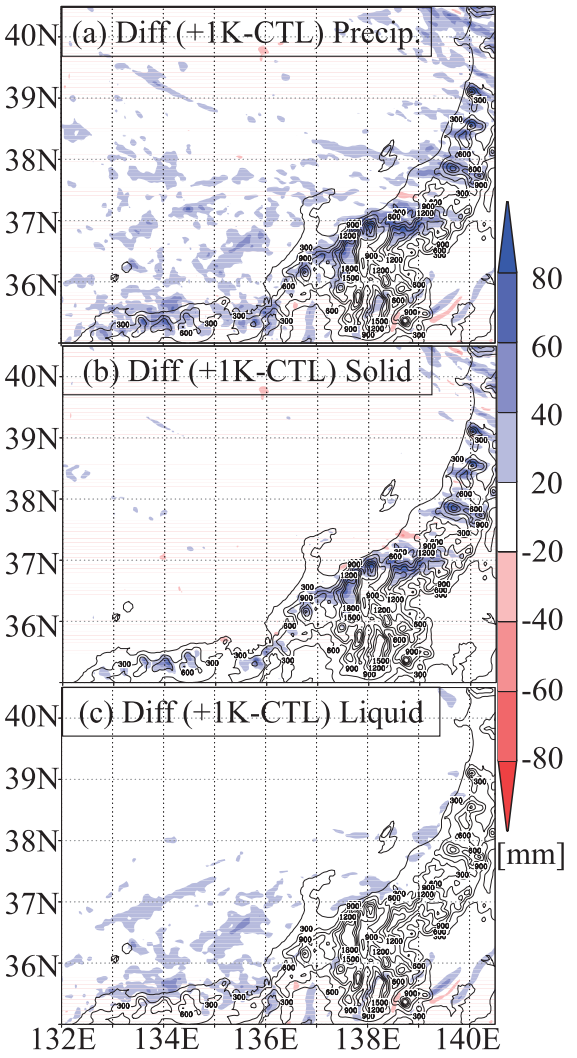

Fig. 3. Differences in monthly accumulated (a) total, (b) solid, and (c) liquid precipitation between CTL and SST + 1K for January 2006 (SST + 1K minus CTL). Blue (red) indicates a positive (negative) signal. The unit is millimeters per month. The solid contours over the land represent orography of 300, 600, 900, 1200, 1500, and 1800 m in the numerical model.

experiments for December 2005 and February 2006. The SST + 1K and SST + 2K experiments calculate more precipitation than did the CTL over the entire domain (Fig. 3), while SST − 1K showed a decrease in precipitation over the entire domain (not shown). Hence, the results suggest that the precipitation over the Japan Sea side of Japan is positively correlated with the SST in the Japan Sea. The increase in precipitation on the Japan Sea side is likely to be associated with changes in latent heat flux over the Japan Sea though air mass modification processes because the air mass is very dry over the Eurasian continent.

Spatially, compared to CTL, SST + 1K showed increases in solid precipitation over the Japan Sea side of the Tohoku District and the relatively higher mountainous areas where the monthly surface air temperature was lower than approximately 0–2°C (not shown), while increases in liquid precipitation were calculated over the Chugoku District (Fig. 3). Solid and liquid precipitations were computed by the microphysics scheme.

To understand whether the changes in precipitation consist of a small number of extreme precipitation events or a large number of individual precipitation events, the time series of accumulated precipitation over the Hokuriku District is shown in Fig. 4. The precipitation was averaged over reference region 1 (Fig. 1). If the development of cloud-precipitation systems dramatically changed owing to warmer SST, the shapes of time series in accumulated precipitation would be different among CTL and the sensitivity experiments. However, the differences in the domain-averaged precipitation among CTL, SST + 1K, SST + 2K, and SST − 1K widen gradually, which implies that precipitation increased in many individual precipitation events. The shapes of time series of accumulated precipitation in CTL and sensitivity experiments were similar. This indicates that dramatic changes in cloud-precipitation systems and atmospheric circulation did not occur in our experiments, in which SST changed in the range of −1 to 2 K. Therefore, the increase in precipitation on the Japan Sea side that is related to the SST warming is distinct.

The sensitivity of precipitation to SST in December 2005 and February 2006 in the series of experiments with FNL and OISST was very similar to that for January 2006 (previously illustrated), which indicates that similar sensitivities can be obtained under different boundary conditions. In addition, we conducted an additional set of experiments by forcing different initial and boundary conditions, which are described in Appendix A. These experiments driven by different boundary conditions showed the same sensitivities of precipitation on the Japan Sea side to SST in the Japan Sea which indicates that the sensitivity is very robust, although the absolute value of sensitivity in an experiment may depend on the model. We discuss the physical mechanism that quantitatively determines the sensitivity in Section 4. Quantitatively, the rate of increase in precipitation per

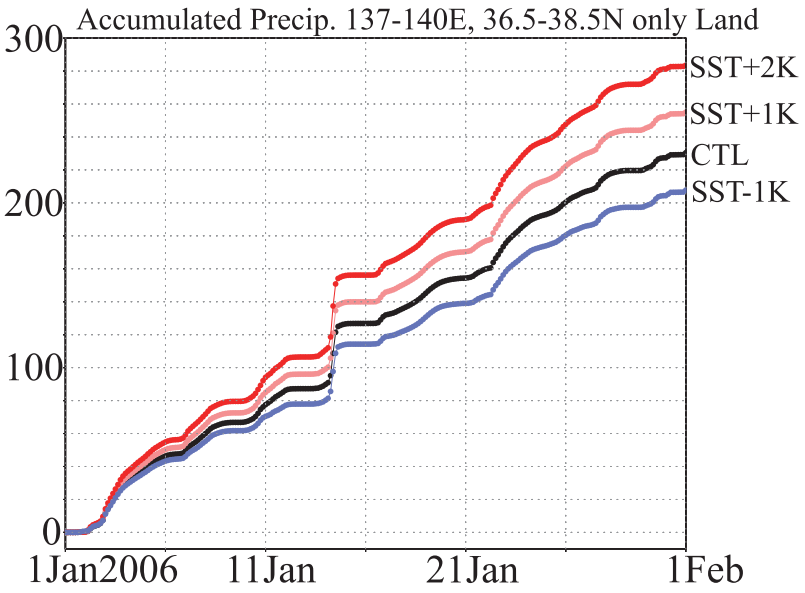

Fig. 4. Time series of simulated precipitation over the reference region 1 (137–140°E, 36.5–38.5°N; shown in Fig. 1), except for the ocean. Black, pink, red, and light-blue lines indicate CTL, SST + 1K, SST + 2K, and SST − 1K, respectively. The precipitation was accumulated from 00 UTC 1 January 2006. The unit is millimeters.

Table 2. (a) The three upper lines indicate simulated monthly precipitation over the land in reference region 1 (137–140°E, 36.5–38.5°N; shown in Fig. 1). (b) The three lower lines denote the over-land region of the whole inner domain (132–140.5°E, 35–40.5°N). The unit is millimeters per month. The values in the parentheses indicate the increase ratio of averaged precipitation, as explained in parentheses in the table heading. The unit is percentage.

(a)	SST − 1K	CTL (CTL/ − 1K)	SST + 1K (+1K/CTL)	SST + 2K (+2K/ +1K)
DEC2005	329.9	358.2 (8.6%)	397.8 (11.1%)	433.3 (8.9%)
JAN2006	207.7	230.4 (10.9%)	255.0 (10.7%)	283.5 (11.2%)
FEB2006	187.3	198.6 (6.0%)	216.3 (8.9%)	228.5 (5.6%)
(b)	SST − 1K	CTL (CTL/ − 1K)	SST + 1K (+1K/CTL)	SST + 2K (+2K/ +1K)
DEC2005	196.8	217.3 (10.5%)	242.3 (11.5%)	268.8 (10.9%)
JAN2006	140.2	153.5 (9.5%)	168.7 (9.9%)	185.5 (9.9%)
FEB2006	160.9	170.0 (5.6%)	182.2 (7.2%)	191.6 (5.2%)

1 K SST warming in December, January, and February was 6–12% over reference region 1 (Tables 2 and A1). Moreover, the rate of increase in precipitation per 1 K of SST warming over the entire land region of the inner domain was 6–12%, which almost corresponds with that of the reference region.

3.3 Increase in latent heat flux over the Japan Sea

To quantitatively understand the precipitation changes related to the SST warming, we examined changes in latent heat flux over the Japan Sea. Because the air mass is very dry over the Eurasian continent, the source of water vapor for precipitation on the Japan Sea side must be the latent heat flux over the Japan Sea. The latent heat flux increased 11–14% over the entire domain over the Japan Sea between CTL and SST + 1K (Fig. 5). Larger rates of increase in latent heat flux were found over the western Japan Sea. The

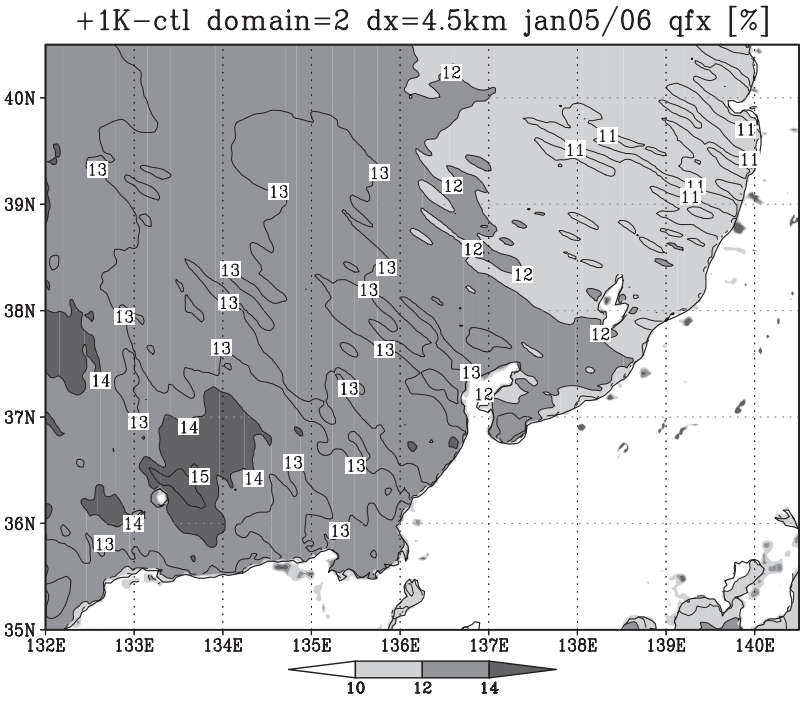

Fig. 5. Differences in the simulated monthly mean latent heat fluxes between CTL and SST + 1K in domain 2. The differences are shown in percentage relative to the values of CTL.

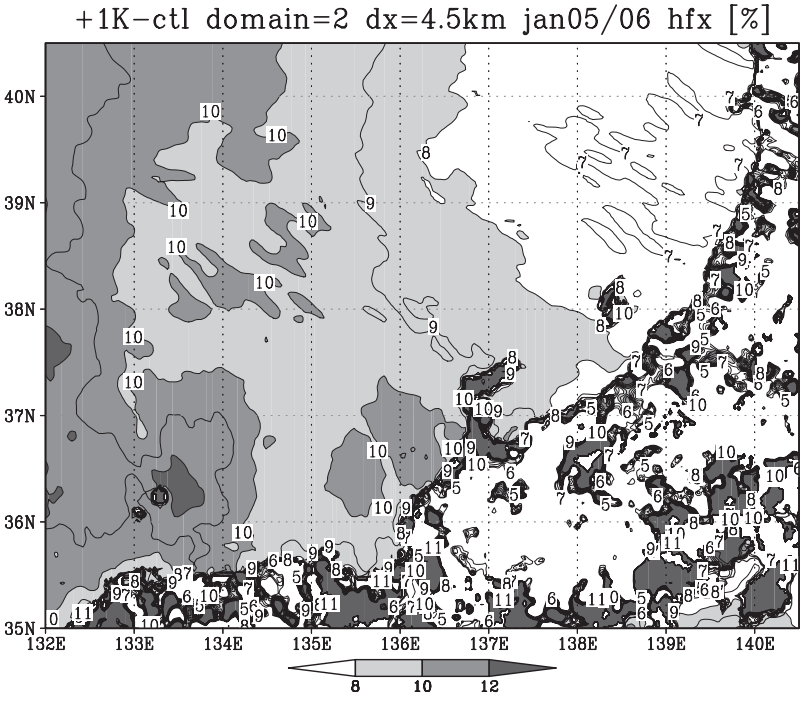

Fig. 6. Differences in the simulated monthly mean sensible heat fluxes between CTL and SST + 1K in domain 2. The differences are shown in percentage relative to the values of CTL.

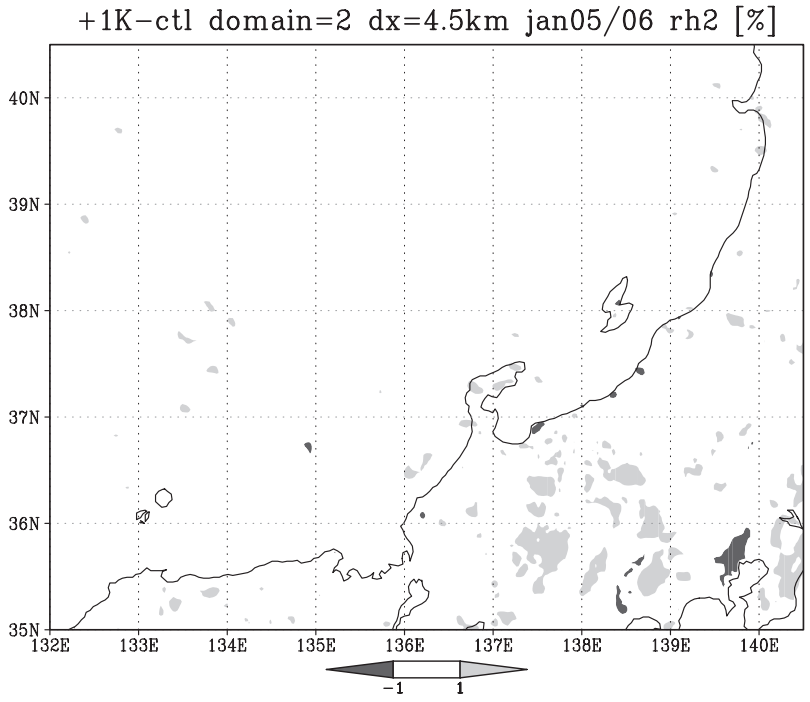

Fig. 7. Differences in the simulated monthly mean surface relative humidity between CTL and SST + 1K in domain 2. The unit is percentage.

increases in rates of latent heat flux were basically the same or relatively larger than the increases in precipitation over the Japan Sea side of Japan (Table 2). The sensible heat flux increased by 7–11% with a 1 K SST warming over the Japan Sea (Fig. 6). A larger increase in sensible heat flux was calculated over the western Japan Sea. As shown in Fig. 7, the differences in relative humidity between CTL and SST + 1K at 2 m above the surface over the entire domain were within − 1% to 1%. Thus, changes in the SST caused small changes in relative humidity. The small changes in relative humidity are consistent with the correspondence between the increases in latent heat flux and precipitation, which indicates that the increased water vapor was used to precipitation. With a 1 K increase in SST, surface air warming was calculated to increase by 0.4–0.6 K (Fig. 8). The increase in surface air temperature was larger over the northwestern coast of Honshu (Japan's main Island). The increase in surface air temperature over the Japan Sea coast was 0.6 K, which was smaller than the prescribed 1 K SST warming. The increase in surface air temperature over the Japan Sea coast may be associated with the accumulated effects of sensible heat flux over the Japan Sea because the warming of surface air temperature over the Japan Sea gradually increased toward Honshu. If the Japan Sea was wider, the warming in surface air temperature would be close to 1 K.

A general explanation for the increase in precipitation with SST warming is that the amount of water vapor increases while the relative humidity is unchanged. The holding capacity of water vapor in the air increases by approximately 7% K^{-1} of warming and is governed by the Clausius–Clapeyron (CC) equation. Because the water vapor amount also increases by approximately 7% K^{-1} of warming under the condition of unchanged relative humidity, the calculated precipitation is basically explained by the equation. However, the increase in latent heat flux was larger than the CC effect of approximately 7%.

The bulk formula can help in the understanding of the larger increase in latent heat flux compared with the CC effect:

$$l E = l\rho\beta C_H U(q_{SAT}(T_S) - q) \quad (1)$$

where l is heat of vaporization, E is amount of evaporation, ρ is the density of air, β is an efficiency of evaporation, C_H is a constant of mixing, U is the wind velocity, T_S is the surface temperature, q_{SAT} is the

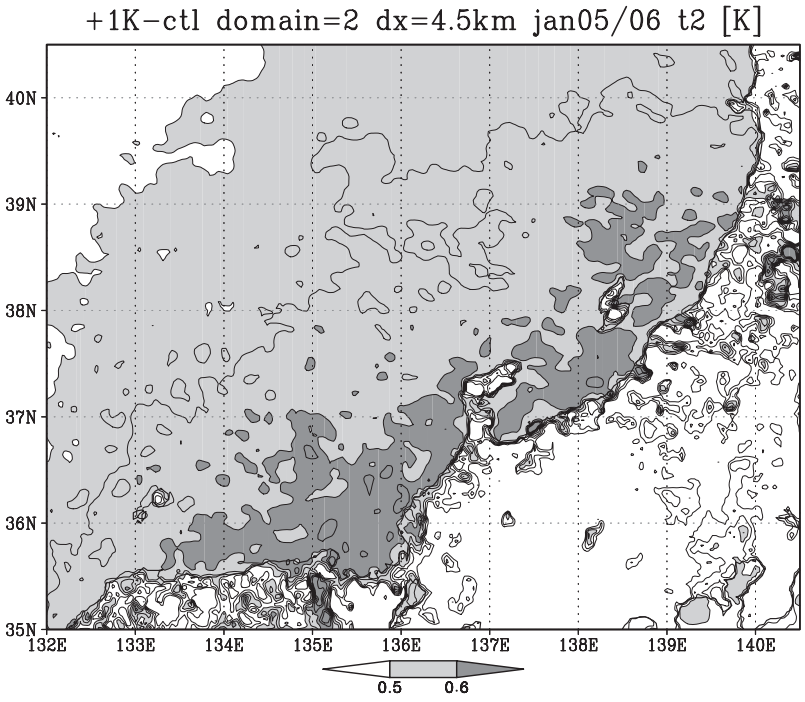

Fig. 8. Differences in the simulated monthly mean surface air temperature between CTL and SST + 1K in domain 2. The unit is Kelvin.

Table 3. Monthly mean simulated values over reference region 2 (133–137°E, 37.5–39.5°N; shown in Fig. 1). Reference region 2 is located on the windward side of reference region 1 (Fig. 1). *V* , *q2m*, *lE*, *H*, *PBLH*, *PW*, *T2m*, and *RH2m* are wind velocity at the lowest layer of the model, specific humidity (2 m), latent heat flux, sensible heat flux, height of the planetary boundary layer, precipitable water, surface air temperature (2 m), and surface relative humidity (2 m), respectively. These values are expressed in m s^{-1}, g kg^{-1}, W m^{-2}, W m^{-2}, m, mm, K, and %, respectively. The values in parentheses for the upper six components indicate the increase in the ratio of the averaged values, as explained in parentheses in the first row of the table. The unit is percentage. For *T2m*, the values in parentheses are the differences between SST − 1K and CTL, between CTL and SST + 1K, and between SST + 1K and SST + 2K, as shown by the eighth row of the table.

	SST − 1K	CTL (CTL/ − 1K)	SST + 1K (+1K/CTL)	SST + 2K (+2K/ +1K)
V (m s^{-1})	9.11	9.36 (2.78%)	9.59 (2.40%)	9.83 (2.48%)
q2m (g kg^{-1})	3.27	3.41 (4.26%)	3.55 (4.21%)	3.70 (4.24%)
lE (W m^{-2})	146.27	165.74 (13.31%)	186.89 (12.76%)	210.31 (12.53%)
H (W m^{-2})	121.07	133.28 (10.09%)	145.73 (9.33%)	158.87 (9.02%)
PBLH (m)	813	852 (4.77%)	888 (4.16%)	921 (3.67%)
PW (mm)	5.83	6.02 (3.33%)	6.22 (3.33%)	6.43 (3.30%)
	SST − 1K	CTL (CTL- − 1K)	SST + 1K (+1K-CTL)	SST + 2K (+2K-+1K)
T2m (K)	274.69	275.23 (0.55 K)	275.78 (0.54 K)	276.31 (0.54 K)
RH2m	77.08	77.31	77.54	77.82

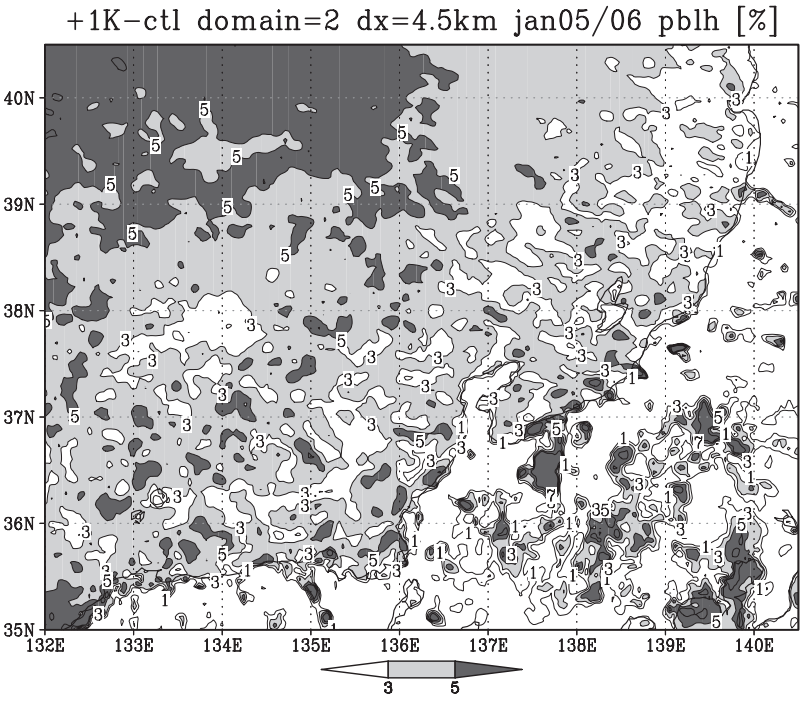

Fig. 9. Differences in the simulated monthly mean planetary boundary layer height between CTL and SST + 1K in domain 2. The differences are shown in percentage relative to the values of CTL.

saturated specific humidity at T_S, and q is the specific humidity of the lower atmosphere. Here β equals 1 over water and T_S is the SST over the Japan Sea. Thus, the latent heat flux is determined by the wind velocity and the difference between the saturated specific humidity at SST and the surface specific humidity.

Because CTL and the sensitivity experiments were forced by the same atmospheric boundary conditions every 6 h, changes in wind patterns were small. As shown in Fig. 4, there were no drastic changes in the precipitation events, which supports our abovementioned suggestion that drastic changes in atmospheric circulation, such as extratropical cyclones, did not occur. We confirmed the changes in wind velocity at the lowest layer of the model among the series of experiments and found that the rate of increase in the monthly simulated surface wind velocity over reference domain 2 (Fig. 1) was 2.4–2.8% per 1 K of SST warming (Table 3). The increase in surface wind velocity probably contributed to the increase in latent heat flux. The increase in wind velocity can be explained by the increase in latent heating associated with the increase in precipitation on the Japan Sea side and the increase in vertical mixing due to the development of planetary boundary layer (see Section 4.1). The anomalous atmospheric circulation was very similar to the changes in water vapor flux, which are shown in Fig. 12.

The CC equation yields an approximately 7% increase when both SST and surface air temperature increase by 1 K. However, because the increase in surface air temperature was less than 1 K and relative humidity was unchanged, the rate of increase in q between CTL and SST + 1K must be smaller than 7%, which can be confirmed from Table 3. Hence, the term $(q_{SAT}(T_S) - q)$ must be larger than that in the case in which both SST and surface air temperature increased by 1 K. Therefore, the 11–14% increase in latent heat flux, which is larger than a theoretical estimation of approximately 7% from the CC equation, is physically consistent with the changes estimated by the bulk formula. The deviation of latent heat flux from the CC equation estimation of 7% is quantitatively discussed in Section 4.

4. Discussion

4.1 Development of planetary boundary layer

In Section 3.3, we found that the increase in latent heat flux due to the SST warming was 11–14%, which can be explained by the CC effect and the increase in

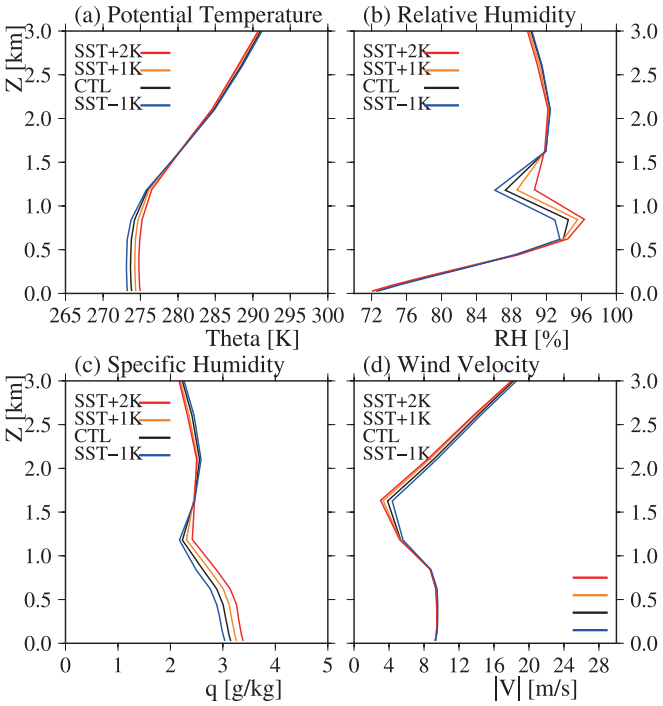

Fig. 10. Monthly mean vertical profiles of (a) potential temperature, (b) relative humidity, (c) specific humidity, and (d) wind velocity averaged over reference region 2 (133–137°E, 37.5–39.5°N; shown in Fig. 1). The unit are K, %, g kg^{-1}, and m s^{-1} respectively.

surface wind velocity. This subsection discusses another effect of the increase in latent heat flux.

To facilitate the following quantitative discussion, the area-averaged values over reference region 2 are summarized in Table 3. The sensible heat flux increased from 7% to 11% as a result of SST warming. An increase in sensible heat flux can result in the development of a planetary boundary layer over the Japan Sea. This development of the planetary boundary layer is a potential cause of the increase in sensible and latent heat fluxes over the Japan Sea. Mixing in the planetary boundary layer results in upward transport of water vapor, which leads to a decrease or maintenance of low values of water vapor near the surface. In addition, the effect simultaneously suppresses the warming of surface air temperature, which increases the sensible heat flux because of the increased difference between the surface air temperature and SST. As a consequence, the height of the planetary boundary layer increases because of the increased sensible heat flux. The development of the height of the planetary boundary layer over the Japan Sea was calculated to be 3–5%, as shown in Fig. 9. The development of the planetary boundary layer was also confirmed by Fig. 10.

Because water vapor is well-mixed in the planetary boundary layer, a taller planetary boundary layer can hold more water vapor. The air mass above the planetary boundary layer is dry, and thus, the rate of development of the height of the planetary boundary layer may correspond to the rate of increase in water vapor content in the planetary boundary layer under the condition that relative humidity is unchanged. In fact, the area-averaged vertical profiles of relative humidity obtained from CTL and the three sensitivity experiments showed the same condition in the lower planetary boundary layer below 500 m (Fig. 10b). However, large differences in relative humidity were found at approximately 800–1200 m; this height can be considered to correspond to the top of the planetary boundary layer or the bottom of the cloud layer. Therefore, the 3–5% rate of development of the planetary boundary layer can represent the rate of increase in latent heat flux associated with the changes in the planetary boundary layer. Hence, the 11–14% rate of increase in latent heat flux can be explained by the sum of the 7% CC effect and the 3–5% effect from development of the planetary boundary layer, which is

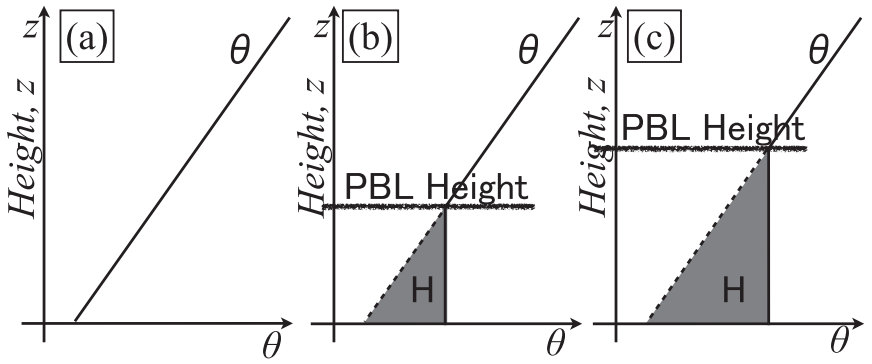

Fig. 11. Development of the planetary boundary layer and its association with sensible heat flux. Solid lines indicate vertical profiles of potential temperature (θ). Dashed lines indicate vertical profiles of potential temperature at the initial condition (a). The shaded area H represents the total amount of heat input to the bottom of the boundary layer (b, c). The development of the planetary boundary layer height is proportional to the one-half power of the sensible heat flux.

equal to 10–12% and is in good agreement with the calculated rate of increase in latent heat flux. This result implies that apart from the CC effect, the effect from the development of the planetary boundary layer is a primary factor in the increase in latent heat flux.

Furthermore, the increase in precipitable water integrated from the surface to the 500-hPa level, from CTL to SST + 1K was 3%, which is comparable to the development of the height of the planetary boundary layer (3–5%). A portion of the water vapor supplied from the Japan Sea could be used for precipitation there. This indicates that our estimation of the increase in precipitable water associated with the development of the planetary boundary layer is also reasonable.

It is noteworthy that these details were common for the CTL experiment and the three sensitivity experiments (Table 3), which indicates that the sensitivity of precipitation associated with changes to SST was robust.

4.2 Theoretical consideration: development of planetary boundary layer

In this subsection, we compare the development of the planetary boundary layer estimated by a theoretical scale analysis with that calculated by a state-of-the-art regional climate model. We show schematics of the development of the planetary boundary layer in Fig. 11. The solid lines indicate vertical profiles of the potential temperature at three stages: the initial condition (Fig. 11a) and the results after the input of a sensible heat flux, H (Figs. 11b and 11c). Gray shading denotes the amount of H from the surface. The initial profile of potential temperature (left panel) is shown by dashed lines. In this case, latent heat release by cloud formation and density changes caused by an increase in absolute amount of water vapor were not considered. Entrainment of high potential temperature air above the planetary boundary layer was also ignored because this effect is one order of magnitude lower than that of the sensible heat flux. As a simple theoretical model, the height of the planetary boundary layer is developed by the sensible heat flux. The rate of increase in the height of the planetary boundary layer is proportional to the rate of increase in the sensible heat flux from the surface to the one-half power:

$$H_{PBL} \propto \sqrt{H} \tag{2}$$

where H_{PBL} is the height of the planetary boundary layer and H is sensible heat flux. Thus, a 7–11% increase in sensible heat flux corresponds to a 2.64% to 3.32% increase in the development of the planetary boundary layer, which closely corresponds to the rate of development of the planetary boundary layer calculated by the state-of-the-art regional climate model. The correspondence between the simple theoretical model and the regional climate model indicates that our simple explanation is qualitatively and quantitatively reasonable.

4.3 Relationship between increases in latent heat flux and precipitation

This subsection investigates why the increase in precipitation on the Japan Sea side of Japan was slightly smaller than the increase in latent heat flux over the Japan Sea. The differences in precipitable water between CTL and SST + 1K indicates an increase in precipitable water over the Japan Sea and also over the leeward side of the Japanese mountain

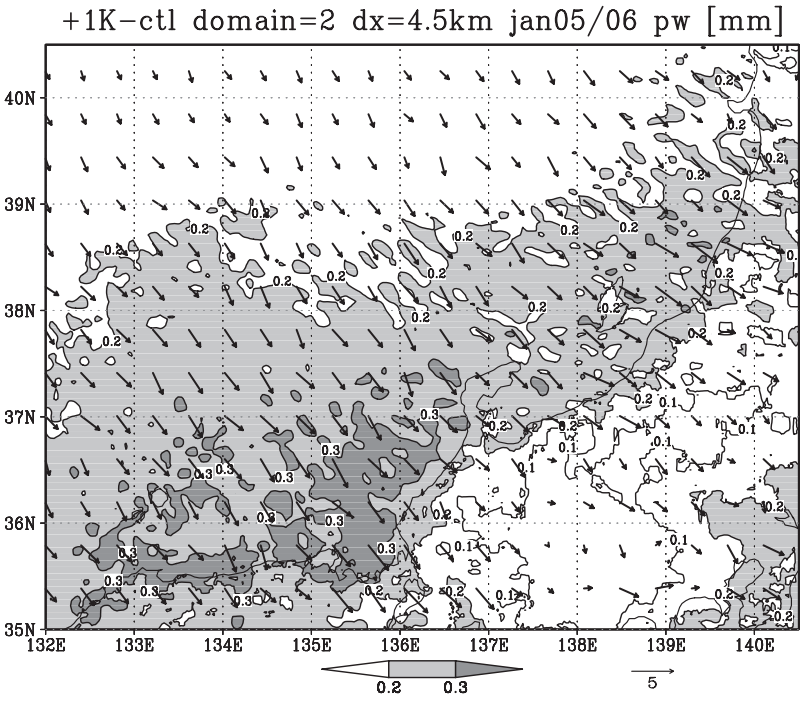

Fig. 12. Differences in the simulated monthly mean precipitable water (shading and contours) between CTL and SST + 1K in domain 2. Vectors indicate differences in the simulated moisture fluxes, which were integrated from the surface to the 500-hPa level. Precipitable water is expressed in mm and moisture fluxes in kg m^{-1} s^{-1}.

range (Fig. 12). Enhanced southeastward vertically integrated moisture fluxes occurred because climatological total moisture fluxes are southeastward. This result indicates that the increase in precipitable water over the leeward side of the Japan's central mountain range was a result of transport from the Japan Sea. The result also indicates some of the increased latent heat flux remains in the atmosphere and is transported to leeward regions. This mechanism can be explained by the increase in holding capacity of water vapor in the air owing to the increased air temperature caused by SST warming. This result is reasonable because the precipitation was mostly associated with orographic forcing. When water vapor is forced upward along the central mountain range, it condenses and precipitation occurs. Therefore, a portion of the increased latent heat flux should remain in the atmosphere.

4.4 Uncertainty in projected precipitation on the Japan Sea side

Here, we discuss the uncertainty in simulated and projected precipitation downscaled from AOGCM output, including uncertainty in SST. AOGCM projections generally include uncertainties. Projected SST has a strong impact on regional and global climate in downscaling experiments, and projections for semi-closed ocean areas such as the Japan Sea have particularly larger uncertainties. Our results may be useful for estimating the uncertainty in simulated and projected precipitation on the Japan Sea side related to the SST uncertainty. Here we use the inter-AOGCM standard deviation as the uncertainty in the AOGCMs. The sensitivity experiments suggested that the increase in precipitation over the Japan Sea side due to a 1 K SST warming over the Japan Sea was approximately 10%. The sensitivity of precipitation to SST can be interpreted as the uncertainty in precipitation associated with the uncertainty in SST. Thus, the uncertainty in precipitation on the Japan Sea side, which is derived from the uncertainty in SST over the Japan Sea, can be estimated as approximately 10% of the total precipitation. This 10% uncertainty corresponds to one-half of the interannual standard deviation in the observed precipitation for a 25-year period from 1983 to 2007 (Table 4). This uncertainty is not small because a 30-year SST change expected with climate change is sufficiently smaller than its interannual variation. Hence, we suggest that the inter-AOGCM uncertainty

Table 4. Observed climatological mean precipitation and its interannual standard deviation for a 25-year period from winter 1982/1983 to 2006/2007 over the land of reference region 1 (137–140°E, 36.5–38.5°N; shown in Fig. 1). The unit is millimeters per month.

	Mean mm/month	Interannual Std (AMeDAS) mm/month	(Std/Mean) × 100 %
DEC	220.0	51.4	23.4
JAN	221.9	47.5	21.4
FEB	155.0	35.4	22.8

for the Japan Sea should be considerably smaller than 1 K.

5. Conclusion

This study addressed the impact of SST in the Japan Sea on the winter precipitation on the Japan Sea side of Japan. To understand this impact, a CTL and three sensitivity experiments using the same initial and boundary conditions, except for SST, were conducted for December 2005, January 2006, and February 2006 using a high-resolution regional model.

The spatial pattern of the monthly precipitation for the CTL simulation was in close agreement with the observations. The seasonal progression of the simulated precipitation was confirmed with two types of observations, which indicates that the 4.5-km resolution model realistically captured spatial–temporal variations in precipitation over the Japan Sea side of Japan in the CTL simulation.

The simulated precipitations amounts of SST + 1K and SST + 2K were larger than those of CTL, but those of SST−1K were lower, which indicates that the exponential increases in precipitation related to SST warming are very robust. Therefore, we concluded that the precipitation on the Japan Sea side increases exponentially with SST warming over the Japan Sea. The rate of increase in precipitation per 1 K increase in SST is 6–12% over the Hokuriku District. The 11–14% increase in latent heat flux over the Japan Sea was in close agreement with the increase in precipitation. The increase in latent heat flux can be quantitatively explained by a CC-equation contribution of 7% and an effect of development of planetary boundary layer contribution of 3–5%. The development of the planetary boundary layer caused by the SST warming reasonably corresponded to the increase in sensible heat flux. In addition, the rate of increase in the height of the planetary boundary layer almost corresponded with the rate of increase in precipitable water. It is noteworthy that a portion of the increased water vapor remained in the atmosphere and was transported leeward, which was associated with the increase in holding capacity of water vapor in the atmosphere owing to warming of the atmosphere. The rest of the increase in latent heat flux was partly explained by the increase in surface wind velocity, which could be the result of increased latent heating from precipitation on the Japan Sea side. Finally, this study also proposes that an uncertainty of 1 K in SST simulated and projected by multiple AOGCMs in the Japan Sea corresponds to an uncertainty in precipitation of approximately 10% on the Japan Sea side.

Appendix A

We also examined whether the sensitivity of precipitation to SST was dependent on the atmospheric and SST conditions used as boundary conditions. To test this, we used another set of experiments driven by different initial and boundary conditions. The ERA-Interim product (Berrisford et al. 2009) of the European Centre for Medium-Range Weather Forecasts (ECMWF) was used as atmospheric and SST initial and boundary conditions. The experimental design was the same as for CTL and SST + 1K, SST + 2K, and SST − 1K, except for the initial and boundary conditions, which are referred to as ERA-CTL, ERA-SST + 1K, ERA-SST + 2K, and ERA-SST − 1K, respectively. The spatial distribution of the prescribed SST from ERA-CTL is shown in Fig. A1. The large-scale distribution was similar, but the SST values were extremely low, which are probably artificial interpolation errors that occurred near the coast. However, this was a good examination of the robustness of the sensitivity of precipitation to SST. In addition, we compared the simulated monthly mean wind fields at 850 hPa in January 2006 between CTL and ERA-CTL (Figs. A2 and A3). Although the wind velocity was stronger in ERA-CTL, the large-scale patterns were the same. Both atmospheric circulation fields showed the typical Asian winter monsoon pattern.

The differences between ERA-CTL and ERA-SST + 1K for January 2006 are shown in Fig. A4. Spatially,

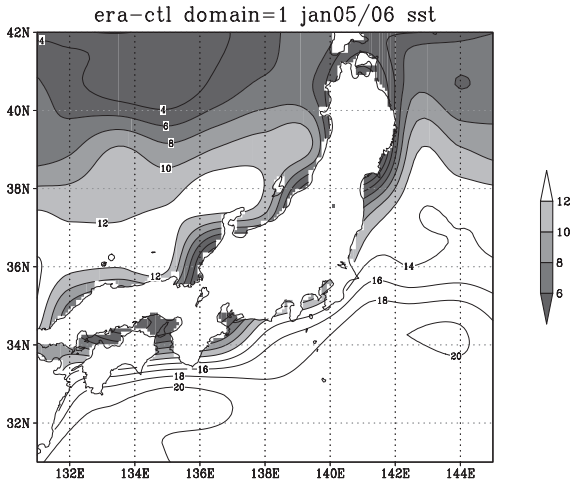

Fig. A1. Prescribed SST from ERA-CTL. SSTs were produced for ERA-SST + 1K, ERA-SST + 2K, and ERA-SST − 1K and were based on the SST in ERA-CTL.

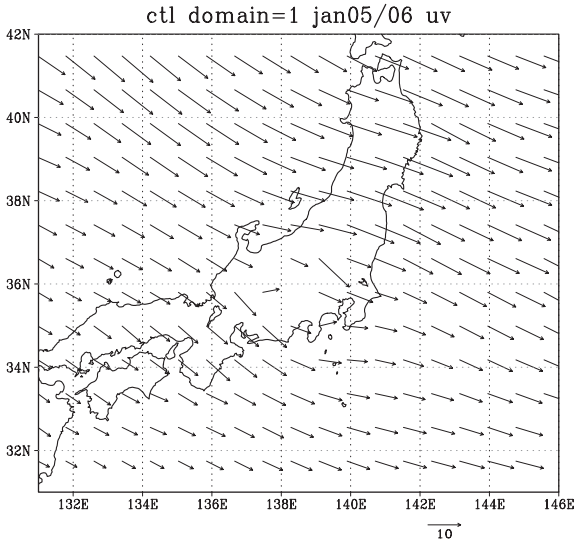

Fig. A2. Simulated monthly mean wind field at 850 hPa from CTL. The wind vectors were plotted for every 10 vectors in longitude and latitude.

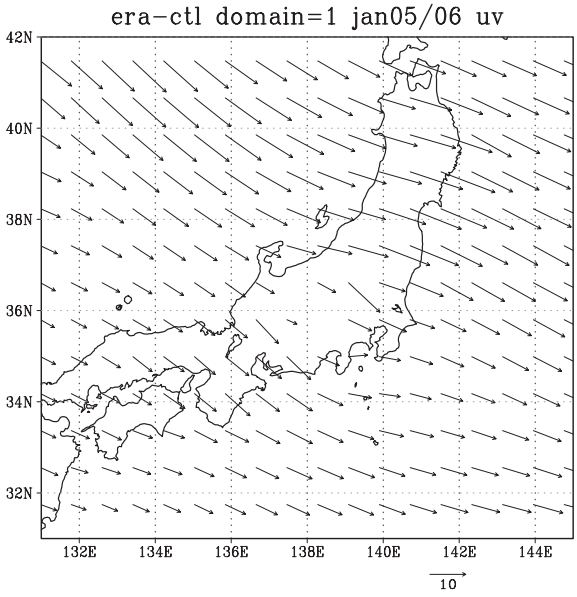

Fig. A3. Same as Fig. A2, but for ERA-CTL.

compared to CTL, SST + 1K showed increases in solid precipitation over the Japan Sea side of the Tohoku District and the relatively higher mountainous areas, whereas increases of liquid precipitation were calculated over the Chugoku District (Fig. A4). This result was consistent with the series of experiments with FNL and OISST. These differences in precipitation were in good agreement with the differences between ERA-SST + 1K and ERA-SST + 2K and between ERA-SST − 1K and ERA-CTL. In addition, similar results were obtained from the experiments for December 2005 and February 2006. We also show Fig. A5, which was same as Fig. 4 but for the different set of experiments with ERA-Interim. The differences in the domain-averaged precipitation among ERA-CTL, ERA-SST + 1K, ERA-SST + 2K, and ERA-SST − 1K widen gradually, which implies that precipitation increased in many individual precipitation events. The shapes of time series of accumulated precipitation were similar among ERA-CTL, ERA-SST + 1K, ERA-SST + 2K, and ERA-SST − 1K. These results are consistent with those obtained from CTL, SST + 1K, SST + 2K and SST − 1K. Thus, the sensitivity of precipitation over the Japan Sea side of Japan to SST over the Japan Sea was robust.

The results of ERA-CTL and the three sensitivity experiments driven by ERA-Interim are summarized in Tables A1 and A2. Although the absolute values of precipitation and sea surface fluxes were different, the sensitivity of precipitation to SST was basically the same. The calculated precipitation on the Japan Sea

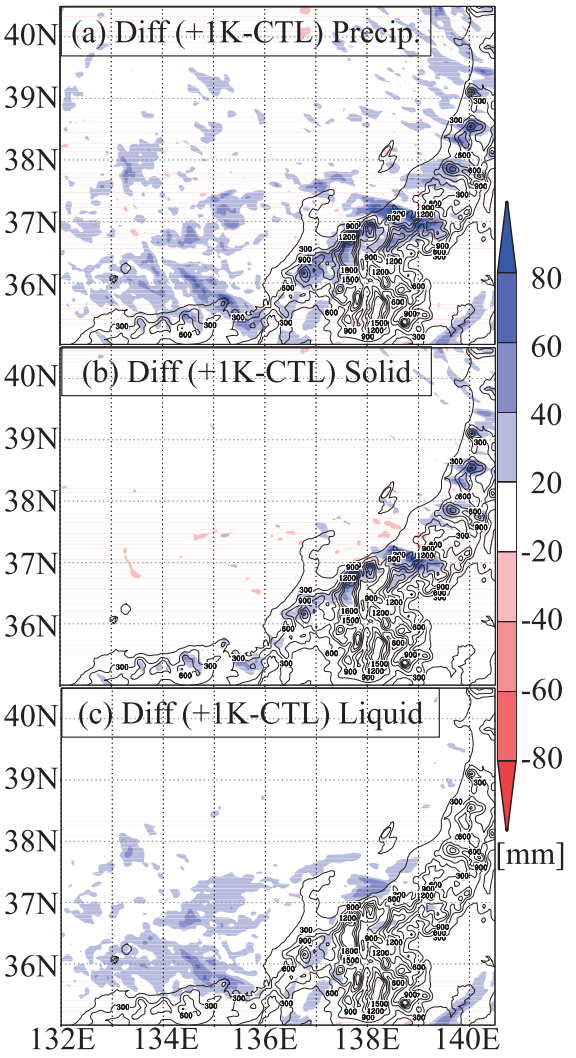

Fig. A4. Differences in monthly accumulated (a) total, (b) solid, and (c) liquid precipitation between ERA-CTL and ERA-SST + 1K for January 2006 (ERA-SST + 1K minus ERA-CTL). Blue (red) indicates a positive (negative) signal. The unit is millimeters per month. The solid contours over the land represent orography of 300, 600, 900, 1200, 1500, and 1800 m in the numerical model.

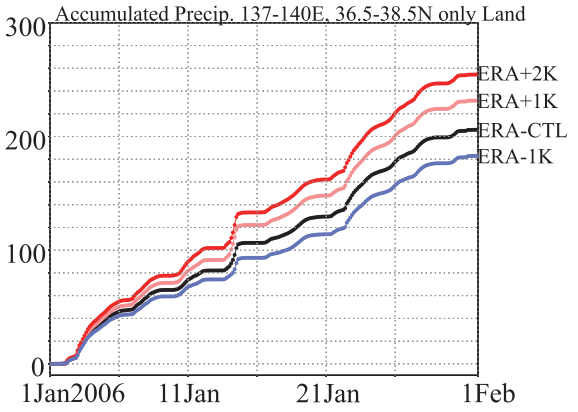

Fig. A5. Time series of simulated precipitation over reference region 1 (137–140°E, 36.5–38.5°N; shown in Fig. 1), except for the ocean. Black, pink, red, and light-blue lines indicate ERA-CTL, ERA-SST + 1K, ERA-SST + 2K, and ERA-SST − 1K, respectively. The precipitation was accumulated from 00 UTC 1 January 2006. The unit is millimeters.

side increased by 6–14% K^{-1} of SST warming. In addition, the related physical values, such as latent heat flux, sensible heat flux, and planetary boundary layer height, were larger than those of CTL and the three sensitivity experiments driven by FNL and OISST, which is consistent with the larger precipitation amounts in the experiments driven by ERA-Interim. The sensitivities of precipitation to SST in December 2005 and February 2006 driven by ERA-Interim were also basically the same as those from FNL and OISST. The correspondence of the sensitivity of precipitation on the Japan Sea side to SST over the Japan Sea with different initial boundary conditions implies the robustness of our results.

Acknowledgments

We thank two anonymous reviewers for their helpful suggestions and comments. FNL data were downloaded from http://dss.ucar.edu/datasets/ds083.2/. NOAA OISST V2 data were provided by the NOAA/OAR/ESRL PSD, Boulder, Colorado, USA, from their website at http://www.esrl.noaa.gov/psd/. This study was partly supported by the Research Program on Climate Change Adaptation (RECCA) Fund and the “Green Network of Excellence (GRENE)” program by the Ministry of Education, Culture, Sports, Science, and Technology (MEXT), Japan.

Table A1. (a) The three upper lines indicate simulated monthly precipitation driven by ERA-Interim over land in reference region 1 (137−140°E, 36.5–38.5°N; shown in Fig. 1). (b) The three lower lines denote the over-land region of the whole inner domain (132–140.5°E, 35–40.5°N). The unit is millimeters per month. The values in parentheses indicate the increase in the ratio of averaged precipitation, as explained in parentheses in the table heading. The unit is percentage.

(a)	SST − 1K	CTL (CTL/ − 1K)	SST + 1K (+1K/CTL)	SST + 2K (+2K/ +1K)
DEC2005	395.0	436.3 (10.5%)	490.3 (12.4%)	541.4 (10.4%)
JAN2006	183.2	206.1 (12.5%)	231.8 (12.5%)	254.8 (9.9%)
FEB2006	184.0	198.4 (7.8%)	213.5 (7.6%)	233.6 (9.4%)
(b)	SST − 1K	CTL (CTL/ − 1K)	SST + 1K (+1K/CTL)	SST + 2K (+2K/ +1K)
DEC2005	228.8	255.5 (11.7%)	285.5 (11.8%)	318.0 (11.4%)
JAN2006	112.5	127.6 (13.4%)	141.3 (10.7%)	155.1 (9.8%)
FEB2006	144.9	154.2 (6.4%)	165.6 (7.4%)	177.0 (6.9%)

Table A2. Monthly physical values for reference region 2 (133−137°E, 37.5–39.5°N) for the series of experiments driven by ERA-interim in January 2006. Reference region 2 is located on the windward side of reference region 1 (Fig. 1). *lE*, *H*, *PBLH*, *PW*, *T2m*, and *RH2m*, are latent heat flux, sensible heat flux, height of the planetary boundary layer, precipitable watert, surface air temperature (2 m), and surface relative humidity (2 m), respectively. These properties are expressed in W m^{-2}, W m^{-2}, m, mm, K, and %, respectively. The values in parentheses for the upper four components indicate the increase in the ratio of the averaged values, as explained in parentheses in the first row of the table. The unit is percentage. For *T2m*, the values in parentheses are the differences between ERA-SST − 1K and ERA-CTL, between ERA-CTL and ERA-SST + 1K, and between ERA-SST + 1K and ERA-SST + 2K, as shown in the seventh row.

	ERA-SST − 1K	ERA-CTL (CTL/ − 1K)	ERA-SST + 1K (+1K/CTL)	ERA-SST + 2K (+2K/ +1K)
lE (W m^{-2})	189.5	212.4 (12.1%)	238.8 (12.4%)	266.8 (11.7%)
H (W m^{-2})	154.8	167.8 (8.4%)	182.3 (8.6%)	196.6 (7.8%)
PBLH (m)	831	866 (4.22%)	896 (3.66%)	930 (3.58%)
PW (mm)	5.82	6.02 (3.44%)	6.22 (3.35%)	6.44 (3.42%)
	ERA-SST − 1K	ERA-CTL (CTL- − 1K)	ERA-SST + 1K (+1K-CTL)	ERA-SST + 2K (+2K-+1K)
T2m (K)	275.17	275.72 (0.55 K)	276.25 (0.53 K)	276.79 (0.54 K)
RH2m	78.22	78.65	79.05	79.39

References

Chen, F., and J. Dudhia, 2001: Coupling an advanced land surface-hydrology model with the Penn State-NCAR MM5 modeling system. Part I: Model implementation and sensitivity. *Mon. Wea. Rev.*, **129**, 569–585.

Christensen, J., B. Hewitson, A. Busuioc, A. Chen, X. Gao, R. Held, R. Jones, R. Kolli, W. Kwon, R. Laprise, and others, 2007: Regional climate projections. *Climate Change, 2007: The Physical Science Basis. Contribution of Working groupI to the Fourth Assessment Report of the Intergovernmental Panel on Climate Change*, Cambridge University Press, Cambridge, Chapter 11, 847–940.

Dudhia, J., 1989: Numerical study of convection observed during the winter monsoon experiment using a mesoscale two-dimensional model. *J. Atmos. Sci.*, **46**, 3077–3107.

Hara, M., T. Yoshikane, H. Kawase, and F. Kimura, 2008: Estimation of the impact of global warming on snow depth in Japan by the pseudo-global-warming method. *Hydrol. Res. Lett.*, **2**, 61–64.

Hawkins, E., and R. Sutton, 2009: The potential to narrow uncertainty in regional climate predictions. *Bull. Amer. Meteor. Soc.*, **90**, 1095–1107.

Hirose, N., and K. Fukudome, 2006: Monitoring the Tsushima Warm Current improves seasonal prediction of the regional snowfall. *SOLA*, **2**, 61–63.

Hong, S.-Y., and J. O. J. Lim, 2006: The WRF single-moment 6-class microphysics scheme (WSM6). *J. Korean Meteor. Soc*, **42**, 129–151.

Iizuka, S., 2010: Simulations of wintertime precipitation in the vicinity of Japan: Sensitivity to fine-scale distributions of sea surface temperature. *J. Geophys. Res.*, **115**, D10107, doi: 10.1029/2009JD012576.

Kamiguchi, K., O. Arakawa, A. Kitoh, A. Yatagai, A. Hamada, and N. Yasutomi, 2010: Development of APHRO_JP, the first Japanese high-resolution daily precipitation product for more than 100 years. *Hydrol. Res. Lett.*, **4**, 60–64.

Ma, X., T. Yoshikane, M. Hara, Y. Wakazuki, H. G., Takahashi, and F. Kimura, 2010: Hydrological response to future climate change in the Agano River basin, Japan. *Hydrol. Res. Lett.*, **4**, 25–29.

Manabe, S., 1957: On the modification of air-mass over the Japan Sea when the outburst of cold air predominates. *J. Meteor. Soc. Japan*, **35**, 311–326.

Manabe, S., 1958: On the estimation of energy exchange between the Japan Sea and the atmosphere during winter based upon the energy budget of both the atmosphere and the sea. *J. Meteor. Soc. Japan*, **36**, 123–133.

Mlawer, E., S. Taubman, P. Brown, M. Iacono, and S. Clough, 1997: Radiative transfer for inhomogeneous atmospheres: RRTM, a validated correlated-k model for the longwave. *J. Geophys. Res.*, **102**, 16663–16682.

Nakanishi, M., and H. Niino, 2004: An improved Mellor-Yamada level-3 model with condensation physics: Its design and verification. *Bound. Layer Meteor.*, **112**, 1–31.

Reynolds, R., N. Rayner, T. Smith, D. Stokes, and W. Wang, 2002: An improved in situ and satellite sst analysis for climate. *J. Climate*, **15**, 1609–1625.

Skamarock, W. C., J. B. Klemp, J. Dudhia, D. O. Gill, D. M. Barker, M. G. Duda, X.-Y. Huang, W. Wang, and J. G. Powers, 2008: *A description of the Advanced Research WRF version 3*. NCAR Technical Note NCAR/TN475+STR.

Takahashi, H. G., and T. Idenaga, 2013: Impact of SST on precipitation and snowfall on the Sea of Japan side in the winter monsoon season: Timescale dependency. *J. Meteor. Soc. Japan*, **91**, doi: 10.2151/jmsj.2013-506.

Takano, Y., Y. Tachibana, and K. Iwamoto, 2008: Influences of large-scale atmospheric circulation and local sea surface temperature on convective activity over the Sea of Japan in December. *SOLA*, **4**, 113−116.

Yamamoto, M., and N. Hirose, 2008: Influence of assimilated SST on regional atmospheric simulation: A case of a cold-air outbreak over the Japan Sea. *Atmos. Sci. Lett.*, **9**, 13−17.

Yamamoto, M., and N. Hirose, 2009: Regional atmospheric simulation of monthly precipitation using high-resolution SST obtained from an ocean assimilation model: Application to the wintertime Japan Sea. *Mon. Wea. Rev.*, **137**, 2164−2174.

Yoshikane, T., M. Hara, X. Ma, H. Kawase, and F. Kimura, 2011: Simulated snow water equivalent change between the 1980s and 1990s in the Sea of Japan side area using a regional climate model. *J. Meteor. Soc. Japan*, **89**, 269–282.